

# Clustering of low mass stars around Herbig Be star IL Cep - Evidence of "Rocket Effect" using Gaia EDR3 ?

R. Arun,<sup>1\*</sup> Blesson Mathew,<sup>1</sup> G. Maheswar,<sup>2</sup> Tapas Baug,<sup>3</sup> Sreeja S. Kartha,<sup>1</sup> G. Selvakumar,<sup>2</sup> P. Manoj,<sup>4</sup> B. Shridharan,<sup>1</sup> R. Anusha,<sup>1</sup> Mayank Narang,<sup>4</sup>

<sup>1</sup>Department of Physics and Electronics, CHRIST (Deemed to be University), Bangalore 560029, India

<sup>2</sup>Indian Institute of Astrophysics, Sarjapur Road, Koramangala, Bangalore 560034, India

<sup>3</sup>S.N. Bose National Centre for Basic Sciences, Block-JD, Sector-III, Salt Lake, Kolkata-700106, India

<sup>4</sup>Tata Institute of Fundamental Research, Homi Bhabha Road, Mumbai 400005, India

Accepted XXX. Received YYY; in original form ZZZ

## ABSTRACT

We study the formation and the kinematic evolution of the early type Herbig Be star IL Cep and its environment. The young star is a member of the Cep OB3 association, at a distance of  $798 \pm 9$  pc, and has a "cavity" associated with it. We found that the B0V star HD 216658, which is astrometrically associated with IL Cep, is at the center of the cavity. From the evaluation of various pressure components created by HD 216658, it is established that the star is capable of creating the cavity. We identified 79 co-moving stars of IL Cep at 2 pc radius from the analysis of Gaia EDR3 astrometry. The transverse velocity analysis of the co-moving stars shows that they belong to two different populations associated with IL Cep and HD 216658, respectively. Further analysis confirms that all the stars in the IL Cep population are mostly coeval ( $\sim 0.1$  Myr). Infrared photometry revealed that there are 26 Class II objects among the co-moving stars. The stars without circumstellar disk (Class III) are 65% of all the co-moving stars. There are 9 intense H $\alpha$  emission candidates identified among the co-moving stars using IPHAS H $\alpha$  narrow-band photometry. The dendrogram analysis on the Hydrogen column density map identified 11 molecular clump structures on the expanding cavity around IL Cep, making it an active star-forming region. The formation of the IL Cep stellar group due to the "rocket effect" by HD 216658 is discussed.

**Key words:** stars: variables: T Tauri, Herbig Ae/Be – stars: formation – stars: kinematics and dynamics

## 1 INTRODUCTION

Infrared bubbles or cavity-like structures are ubiquitous in the Milky way (Churchwell et al. 2006, 2007). The formation of the structures is due to the combined effects of radiation (Bisbas et al. 2011), ionization (Sternberg et al. 2003) and stellar winds (Dale et al. 2015) from one or more massive central stars ( $\geq 8 M_{\odot}$ ; Zinnecker & Yorke 2007). The cavities are generally associated with infrared bright rims with high star-forming activity (Morgan et al. 2004). The triggered star formation in the region can create another generation of massive young stars. Fuente et al. (2002) identified cavity structures associated with a sample of Herbig Ae/Be (HAeBe) stars. Thus HAeBe stars and their associated regions are ideal for studying various aspects of triggered star formation.

HAeBe stars are intermediate-mass ( $2-10 M_{\odot}$ ) pre-main sequence (PMS) stars with a circumstellar accretion disk (Herbig 1960; Waters & Waelkens 1998). The dust and gas content in the circumstellar disk/medium produce infrared excess in the spectral energy distribution of HAeBe stars. The recombination emission lines of Hydrogen, Calcium, Iron, etc., are also formed in the disk (Hamann & Persson 1992). From the near-infrared (NIR) imaging studies, Testi et al. (1997, 1998) identified clustering of low mass young stellar objects

(YSO) with HAeBe stars. Also, the spatial density concentration of the low mass YSOs is correlated with the spectral type of the HAeBe star in the center of the distribution (Testi et al. 1999). The YSOs around HAeBe stars are astrometrically associated with the central HAeBe stars (Saha et al. 2020).

IL Cep (also called HD 216629), a B3 spectral type (Merrill & Burwell 1949) and a confirmed PMS star (Assousa et al. 1977; Testi et al. 1994) belongs to Cep OB3 association (Blaauw et al. 1959; Garmany 1973). The star is reported to be associated with the reflection nebula GN 22.51.3 (Magakian 2003). IL Cep belongs to a visual binary system with a companion star HD 216629B at a separation of 7" (Mel'Nikov et al. 1996). Several studies indicate that the star IL Cep itself is an unresolved binary star system consisting of stars having spectral types B3( $\pm 2$ ) and B4( $\pm 2$ ) (Wheelwright et al. 2010; Ismailov et al. 2016). From NIR photometric analysis Testi et al. (1997) found clustering of 24 low mass stars with IL Cep. Later, Fuente et al. (2002) reported cavity formation around IL Cep from the analysis of  $^{13}\text{CO}$  and  $\text{C}^{18}\text{O}$  data. The presence of the cavity is reconfirmed by Zhang et al. (2016). They used  $^{13}\text{CO}$  ( $J = 1 - 0$ ) continuum data and Wide-field Infrared Survey Explorer (WISE) (Cutri et al. 2013) images to define the bounds of the cavity around the IL Cep region. They argue that the violent past of IL Cep created the cavity. Zhang et al. (2016) proposed that the center of the cavity is occupied not by IL Cep but by a slightly more massive star HD

\* E-mail: arun.roy@res.christuniversity.in

216658. Interestingly, [Zhang et al. \(2016\)](#) found that the cavity is not formed due to HD216658. The cavity formation is due to the mass dispersal process triggered by various pressure components of the massive central star in the region. The cavity formation considerably reduces the line of sight extinction towards the region, which gives a unique opportunity to study the clustering using optical Gaia EDR3 data.

The identification of clustering around HAeBe star is not investigated from an astrometric perspective thoroughly. The study carried out by [Saha et al. \(2020\)](#) in the case of the star HD 200775 has shown that 80% of the astrometrically identified co-moving stars are diskless stars (Class III), and spectroscopy of four of them found to show weak  $H\alpha$  emission. As a result, these stars will be missed in NIR and  $H\alpha$  surveys which are classically used to identify the PMS populations. We are using the Gaia Early Data Release 3 (Gaia EDR3) to find the young co-moving stars around IL Cep, thereby identifying clustering of low mass YSOs around Herbig Be stars. Also, we combined infrared photometry and spectroscopic analysis to identify possible disk-bearing stars among the co-moving stars.

The paper is organized as follows. The data used in this study are described in Sect. 2. Sect. 3 explains various analyses carried out for identifying the clustering around IL Cep, identification of disk-bearing stars, and detection of molecular clumps in the region. Also, the possibility of the rocket effect being the initial trigger for the formation of IL Cep and the co-moving stars is given in Sect. 3, and the significant results are summarized in Sect. 4.

## 2 DATA INVENTORY

The Gaia EDR3, made available on 3<sup>rd</sup> December 2020, contains astrometric and photometric data of 1.8 billion sources ([Gaia Collaboration et al. 2020; Lindegren et al. 2020](#)). The astrometric data and three photometric band magnitudes of the stars in the region around IL Cep are taken from Gaia EDR3. The direct conversion of Gaia parallax values has its inherent problems (see [Bailer-Jones et al. 2018](#) for a detailed discussion). [Bailer-Jones et al. \(2020\)](#) estimated the distances of 1.47 billion Gaia EDR3 sources using two methods. The first one is the geometric distance which uses distance likelihood (from Gaia parallax) and a distance prior (an exponentially decreasing space density prior that is based on a Galaxy model) approach, which was also applied in the Gaia DR2 ([Bailer-Jones et al. 2018](#)). The second approach is photogeometric, which uses photometric color and apparent magnitude along with the Gaia parallax. Both the distances show no considerable differences in our sample. Thus we used the geometric distance from [Bailer-Jones et al. \(2020\)](#) for all the stars studied in this work.

The NIR magnitudes used in the analysis are 2MASS J, H, and  $K_S$  ([Skrutskie et al. 2006](#)). Also, the mid-infrared (MIR) magnitudes, IRAC [3.6] and IRAC [4.5], are taken from *Spitzer* Glimpse 360 ([Whitney et al. 2011](#)). We also used the Isaac Newton Telescope (INT) Photometric H-Alpha Survey (IPHAS) ([Drew et al. 2005; Barentsen et al. 2011](#)) magnitudes to identify  $H\alpha$  sources.

The low-resolution optical spectrum of HD 216658, the massive star in the region, and HD 216629B, the visual binary companion of IL Cep, were obtained using the Optomechanics Research (OMR) spectrograph ([Prabhu et al. 1998](#)) mounted on the 2.34 m Vainu Bappu Telescope (VBT), Vainu Bappu Observatory (VBO), Kavalur. The spectra are obtained using the grating centered at the  $H\alpha$  line at 6563 Å. The resolution of the observed spectrum is about 8 Å. The dome flats are obtained for flat fielding the images. The bias subtraction, flat field correction, and spectral extraction are per-

**Table 1.** The table provides log of observation of HD 216658 and IL Cep B

Star	V (mag)	Spectral type	Date of observation	Exposure time (s)
HD 216658	8.9	B0.5V	12-12-2020	1200
IL Cep B	13.8	A6V	26-12-2020	2400

formed with standard IRAF tasks. The wavelength calibration of the spectra was carried out using spectra of FeNe and FeAr calibration lamps. All the extracted raw spectra were wavelength calibrated and continuum normalized using IRAF tasks. For all the stars the average signal-to-noise ratio (SNR) near  $H\alpha$  is above 100. The log of observations of the stars is shown in the [Table 1](#).

The  $^{12}\text{CO}$  ( $J = 1-0$ ) observations of the IL Cep region were retrieved from the Canadian Astronomy Data Centre (CADC). The data is a part of the Canadian Galactic Plane Survey (CGPS) and observed in 1995 using the Five College Radio Astronomy Observatory (FCRAO) 14 m telescope. The data was initially part of the FCRAO Outer Galaxy Survey (OGS; [Heyer et al. 1998](#)). The data has a spatial resolution of 45" and a velocity resolution of 0.15 km s<sup>-1</sup>. The noise level per channel is 0.75 K ( $T^*_R$ ).

## 3 RESULTS

### 3.1 Gaia EDR3 astrometric analysis

In this study, we use the Gaia EDR3 for our astrometric analysis ([Gaia Collaboration et al. 2020](#)). The star IL Cep is at a distance of  $798^{+8}_{-10}$  pc ([Bailer-Jones et al. 2020](#)) and is part of the Cep OB3 association ([Blaauw et al. 1959; Garmany 1973](#)). Clustering of low mass YSOs around the Herbig Be star IL Cep was studied by [Testi et al. \(1998\)](#) using infrared K band observations.

We selected all Gaia EDR3 detections around IL Cep within a radius of 8.5' ( $\sim 2$  pc) and found 1565 sources. We chose 2 pc as our search radius because the core radius of an open cluster is 1-2 pc ([Moraux 2016](#)). This search radius is sufficient to identify clustering, if any, around IL Cep. The detections within our target field are cross-matched with the distance catalog of [Bailer-Jones et al. \(2020\)](#) using EDR3 source ID. We found 1366 matches with distances from [Bailer-Jones et al. \(2020\)](#). Further, the stars with good quality astrometry are selected using the re-normalized unit weight error (RUWE) parameter and an uncertainty cut using the parallax values ([Saha et al. 2020](#)). The stars with  $\text{RUWE} > 1.4$  are avoided due to the Gaia EDR3 astrometry quality recommendations ([Fabricius et al. 2020](#)). And finally, the stars with parallax more than 3-sigma confidence (i.e.  $\text{parallax/error in parallax} > 3$ ) are selected for the analysis. We compiled 477 stars including IL Cep in the 8.5' radius that satisfies the defined astrometric quality criterion as our initial sample for further analysis.

The stars clustered together have been identified by overdensity in the distribution of astrometric parameters ([Castro-Ginard et al. 2020](#)). We used gaussian fitting method on proper motion in right ascension ( $\mu_{\alpha*} = \mu_{\alpha} \cos \delta$ ), proper motion in declination ( $\mu_{\delta}$ ) and distance (d) histograms to check for overdensity of stars around IL Cep. Each of the three histograms showed a single Gaussian distribution. We fitted these histograms with a Gaussian function. The histograms and the fit are shown in [Figure 1](#) (left). The three Gaussian fits provided standard deviation intervals for the three parameters. The standard deviation intervals are shown in the [Figure 1](#) (left). The Gaussian fitting statistics are given in [Table 2](#).

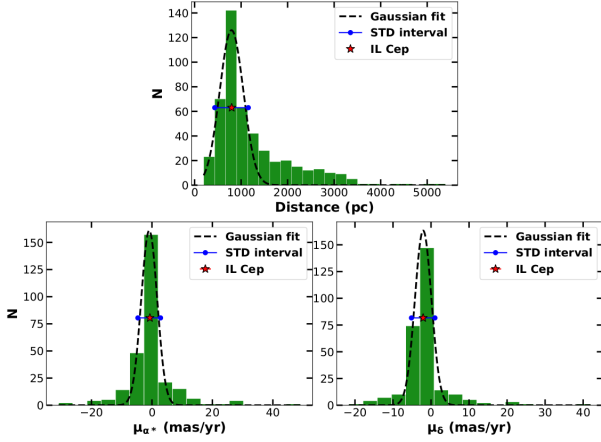


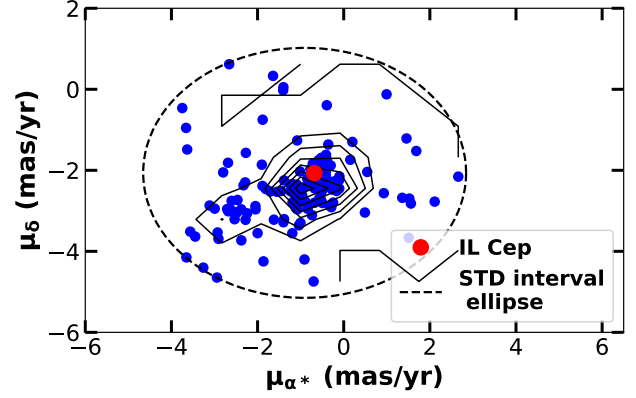
**Figure 1.** The figures show the Gaussian fits on the histograms of distance and proper motion value of stars inside a 2 pc radius around IL Cep and the vector point diagram of "level one" sources. Using the Gaussian fits, we calculated standard deviation intervals for each parameter. IL Cep appears to be inside all three standard deviation intervals, indicating an overdensity of stars around IL Cep. The stars that satisfy the standard deviation intervals are taken as "level one" samples for further analysis. In the vector point diagram, the dashed ellipse is created using the standard deviation intervals of proper motion values. The black contours are the number density contours that indicate an overdensity of stars near IL Cep.

**Table 2.** The table gives the Gaussian fitting statistics of histograms shown in Figure 1 (left).

Astrometric parameter	Mean	Amplitude	Standard Deviation
Distance (pc)	794.0	126.0	360.5
$\mu_{\alpha*}$ (mas yr <sup>-1</sup> )	-0.91	161.0	3.75
$\mu_{\delta}$ (mas yr <sup>-1</sup> )	-2.06	163.3	3.08

IL Cep appears to have an overdensity of stars around it because it is inside the standard deviation intervals of all three parameters. We selected the 165 stars that are inside the standard deviation intervals of all three astrometric parameters. This sample of stars is called the "level one" sample from now. Figure 1 (right) shows the vector point diagram (VPD) of the "level one" sample along with IL Cep. The ellipse shown in the VPD is made using the standard deviation intervals. The number density contours illustrate the overdensity of stars around IL Cep. From the figure, it is clear that there are stars in the "level one" sample that may not be associated with IL Cep. Thus we used the "level one" sample to constrain the astrometric parameters further using a median and median absolute deviation method adopted by Saha et al. (2020). The Gaussian fitting analysis helped us in removing outliers and provided a sample of 165 stars for further analysis. We updated both the parameters to the weighted median (WM) and the weighted median absolute deviation (WMAD). The weights are decided using Gaia G magnitude brightness of the stars. The "weighted" median criterion is adopted due to the increase in the uncertainty of Gaia astrometry with the decrease in the brightness of stars (Gaia Data Release 2 - Documentation release 1.2)<sup>1</sup>.

The WM and WMAD of  $d$  are estimated as 806 pc and 38 pc respectively. The WM and WMAD of  $\mu_{\alpha*}$  is estimated to be -0.91 mas yr<sup>-1</sup> and 0.39 mas yr<sup>-1</sup> respectively. The same for  $\mu_{\delta}$  is given as -2.38 mas yr<sup>-1</sup> and 0.31 mas yr<sup>-1</sup> respectively. Two ellipses are defined using WM and  $3 \times$  WMAD values of  $d$  vs  $\mu_{\alpha*}$  and  $d$  vs  $\mu_{\delta}$ .



The stars that are inside the ellipses are selected as the associated stars of IL Cep (here onwards "level two" sample). Figure 2 shows the  $d$  vs  $\mu_{\alpha*}$  and  $d$  vs  $\mu_{\delta}$  plot with required ellipses. The level one and level two samples are illustrated in the figure. We identified 78 stars from the astrometric analysis, which are clustered around IL Cep inside a 2 pc radius in the sky plane. Figure 3 shows the RGB image of the region made using MIPS 24  $\mu$ m, IRAC 8  $\mu$ m, and IRAC 3.6  $\mu$ m images. The newly identified co-moving stars, IL Cep, and the brightest star in the region, HD 216658 are marked in the *Spitzer* color composite image with the proper motion vectors embedded on them. The proper motion vectors suggest that the selected stars are having similar motion through the sky. The astrometric and photometric data of all 78 co-moving stars are listed in the Table 5

The radius of the region we adopted is 8.5'. To check the possibility of having more co-moving stars in the extended region which is part of the larger star-forming cloud Cep OB3, we checked for stars with similar astrometric constraints in another region near IL Cep. To verify this, we took 8.5' regions 1° south of IL Cep. The number of stars that satisfy the WM and  $3 \times$  WMAD ellipse constraints in the southern region is 5. This shows that even though there may be similar moving stars in the extended regions, there is a clear overdensity of stars that satisfy the astrometric constraints using WM and  $3 \times$  WMAD around IL Cep. The "cavity" defined by Zhang et al. (2016) has a sky area of 0.05 square degrees and the search radius we used has an area of 0.063 square degrees. Both cavity and search radius are shown in Figure 3. The cavity contains 77% of all the co-moving stars, i.e. 60 out of 78 stars are inside the "cavity". This directly implies that there are co-moving stars clustered around IL Cep and the over-density is associated with the cavity.

To summarize, we compiled the stars with high quality astrometric data around IL Cep. Using Gaussian analysis, we filtered out layers and retained 165 stars as level one sample. Finally, using WM and  $3 \times$  WMAD values of the sample we identified a total of 78 co-moving stars of IL Cep.

<sup>1</sup> <https://gea.esac.esa.int/archive/documentation/GDR2/>

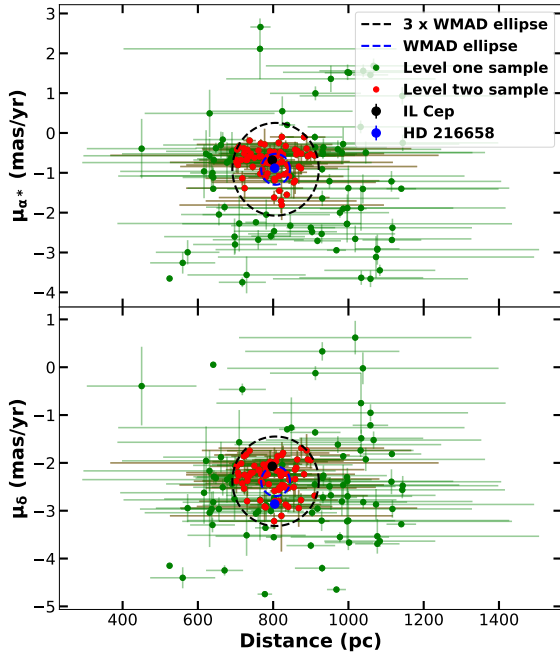


**Figure 2.** The figures show the distribution of selected co-moving stars of IL Cep in  $d$  vs  $\mu_{\alpha^*}$  and  $d$  vs  $\mu_{\delta}$  diagrams. The selected stars are shown using red color star symbols and rejected stars are shown in green. The WM and  $3 \times$  WMAD ellipse are shown in blue and black dashes curves, respectively. IL Cep and HD 216658 are also shown in the figure.

### 3.2 HD 216658 - a massive star astrometrically associated with IL Cep and its co-moving stars

The brightest star in the region of our study is HD 216658, with a  $V$  magnitude of 8.9 mag (Brodskaya 1953). IL Cep is slightly fainter with a  $V$  magnitude of 9.36 mag (Høg et al. 2000). From the literature, it is identified that HD 216658 is of B0-0.5V spectral type (Morgan et al. 1953; Garrison 1970), and IL Cep is of B3 spectral type (Merrill & Burwell 1949). Zhang et al. (2016) suggested that HD 216658 is geometrically positioned at the center of the cavity, but IL Cep is the predominant exciting star in the region. This is quite surprising since HD 216658 is more massive than IL Cep, and hence, should emit more UV flux that can trigger more mass dispersal and create a cavity. We are investigating the possibility of HD 216658 being the cause of cavity formation in the region. From Gaia DR2 estimates HD 216658 is a foreground star at a distance of  $668^{+43}_{-38}$  pc. This is at a distance of 130 pc from IL Cep, which was reported at  $798^{+18}_{-17}$  pc (Bailer-Jones et al. 2018). The RUWE parameter of HD 216658 according to Gaia DR2 data is 2.4, which is significantly higher than the quality cut we gave for the astrometric analysis in Sect. 3.1. Table 3 shows the stellar parameters of IL Cep and HD 216658 either generated in this work or compiled from the literature. In the new data from Gaia EDR3, the star HD 216658 is at a distance of  $807^{+24}_{-24}$  pc, which is similar to the distance of IL Cep, i.e.  $798^{+8}_{-10}$  pc (Bailer-Jones et al. 2020). We saw from the astrometric analysis that HD 216658 is associated with IL Cep and other co-moving stars (Figure 2). The star is excluded from the initial astrometric analysis

**Table 3.** The table provides the stellar parameters of IL Cep and HD 216658 used in this work

Star	$V$ (mag)	Distance (pc)	Spectral type	RUWE
IL Cep	9.4	$798^{+8}_{-10}$	B2-B3	1.0
HD 216658	8.9	$807^{+24}_{-24}$	B0.5V	2.7

due to its high RUWE parameter, which is 2.7 in the Gaia EDR3. The value increased from the last release. Even though the RUWE parameter is high, we can indirectly confirm the association of HD 216658 with the IL Cep co-moving stars and it is part of the Cep OB3 association, which is reported to be at a distance of 800 pc (Moreno-Corral et al. 1993; Pozzo et al. 2003). The distances to the individual members estimated in the pre-Gaia era were in the range of 500-1000 pc (Crawford & Barnes 1970). We took the stars reported as part of the Cep OB3 association by Jordi et al. (1995) and cross-matched them with Gaia EDR3 and extracted the distances from Bailer-Jones et al. (2020). The distance range of the sample was too large (180–9000 pc). Thus we took the stars with distances in the range of 500–1000 pc and found their transverse velocities. The median transverse velocity of the sample is  $11.6 \pm 0.6$  km s<sup>-1</sup>. The transverse velocity of HD 216658 is 11.4 km s<sup>-1</sup> which is similar to the possible members of the Cep OB3 association.

Similarly, the visual binary companion of HD 216658 is named in SIMBAD as HD 216658 B. This is at 6.6" separation from the primary and is a co-moving star candidate in our ‘level two’ sample of IL Cep. Even though the proper motion values of HD 216658 and HD 216658B are shown to be distinct, the transverse velocity of the stars are 11.4 km s<sup>-1</sup> and 11.7 km s<sup>-1</sup> respectively, which is almost identical. Even with the Gaia EDR3 data we cannot confirm that the visual binary of HD 216658 is bounded or not. But with the distance estimates and the transverse velocities, we can indicate that they are both part of the Cep OB3 cloud. This means the Gaia EDR3 distance of HD 216658 is acceptable. Thus we consider the star as a co-moving candidate of Herbig Be star IL Cep.

### 3.3 Two dynamically distinct population among co-moving stars

We estimated the transverse velocity of 79 co-moving stars of IL Cep including HD 216658 using Gaia EDR3 astrometric data. The histogram distribution of the transverse velocities of the stars is shown in Figure 4 (bottom right). The distribution appears to be bimodal, which indicates the presence of two populations of stars among the highly constrained co-moving candidates. The transverse velocity of IL Cep and HD 216658 show that both stars associated with the same cloud, possess different transverse velocities. The bimodal histogram is fitted with a two-gaussian function and the mean velocities of the two populations are found to peak at 8.3 km s<sup>-1</sup> and 11.4 km s<sup>-1</sup>, respectively. This is consistent with the transverse velocity of IL Cep and HD 216658, which are 8.2 km s<sup>-1</sup> and 11.4 km s<sup>-1</sup> respectively. The average uncertainty of the transverse velocity of stars in the analysis is 1.2 km s<sup>-1</sup>. Thus the two populations having a mean velocity difference of 3.2 km s<sup>-1</sup> should be real.

The total stars are classified as two populations, dividing them at a velocity of 10.3 km s<sup>-1</sup> which is the intersection of both Gaussians. Population one is called the HD 216658 population with 24 stars and population two is called the IL Cep population with 56 stars. The IL Cep population constrained by astrometric parameters and transverse



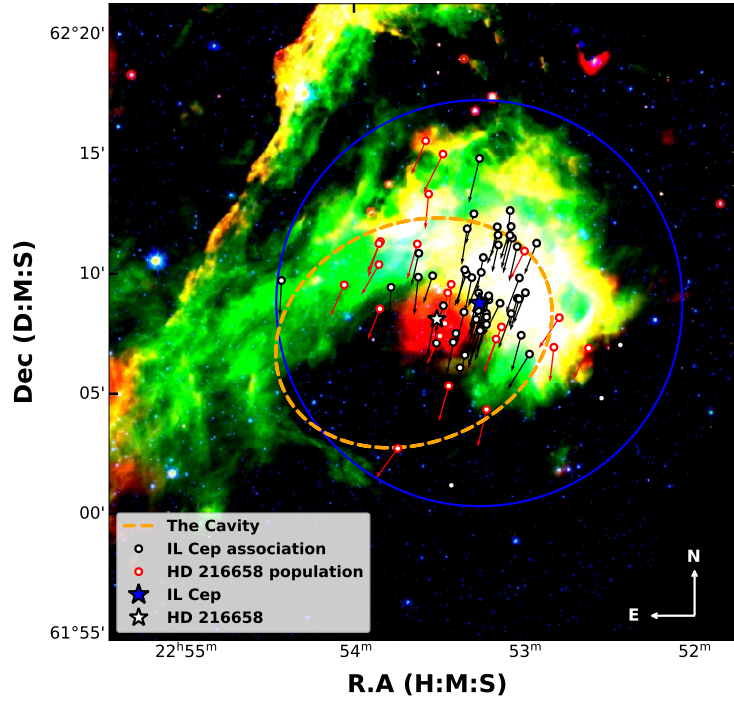


**Figure 3.** The RGB images of the  $25' \times 25'$  region around IL Cep using *Spitzer* (R = MIPS  $24 \mu\text{m}$ , G = IRAC  $8 \mu\text{m}$ , and B = IRAC  $[3.6 \mu\text{m}]$ ) is shown. The brightest star in the region, HD 216658 and IL Cep are marked in the figure. The co-moving stars associated with IL Cep are shown in black encircled symbols and the population associated with HD 216658 is shown in red encircled symbols. The "cavity" defined by Zhang et al. (2016) is shown with a dashed orange ellipse and the 2 pc search radius is shown as a blue circle.

velocity is labeled as "IL Cep stellar group". Both populations are distinctly represented in the Figure 3. The HD 216658 population does not show any preferential clustering around HD 216658 whereas the stars in the IL Cep population seem to be clustered around IL Cep. Figure 4 is additionally showing the histograms made using the distances and transverse velocities of Cep OB3 stars taken from Jordi et al. (1995). The Cep OB3 stars have a distance distribution peaking at 800 pc, which is at a similar distance as the co-moving stars of IL Cep. Also, the transverse velocity distribution of the sample has a median value of  $11.6 \pm 0.6 \text{ km s}^{-1}$ . This is similar to the population of HD 216658. This could indicate that the HD 216658 population is a part of the bigger parent cloud Cep OB3 and IL Cep is a more recent star formation inside the Cep OB3 cloud with a slightly lesser transverse velocity due to some pressure variations inside the parent cloud. From hereon the co-moving stars identified in this study will be treated as two distinct sub-populations associated with HD 216658 and IL Cep, respectively.

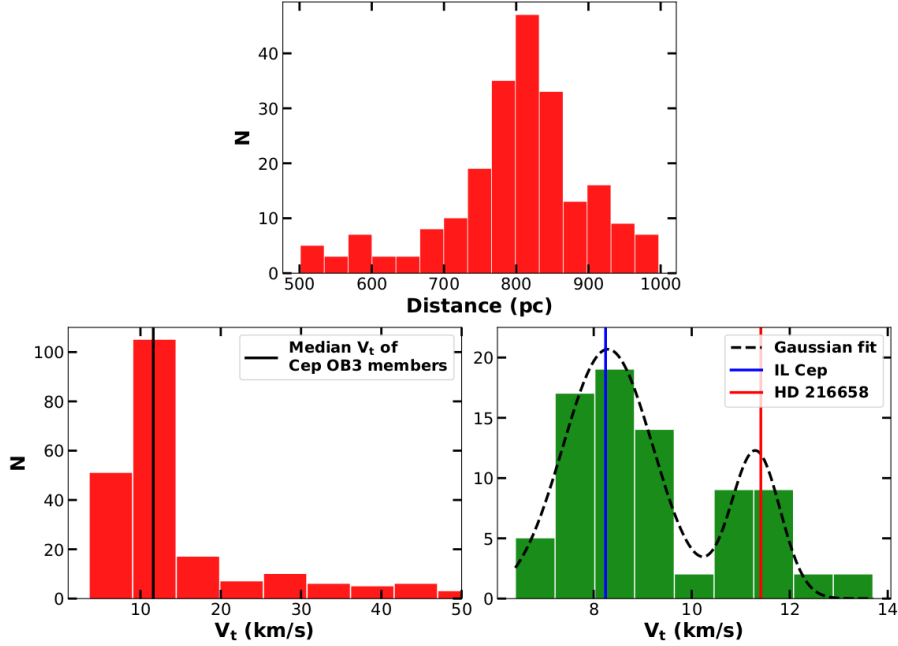
### 3.4 HD 216658 - Central exciting source

The star HD 216658 is found to be astrometrically associated with the IL Cep co-moving stars. The star is at a similar distance as IL Cep. We also identified two populations of stars from the transverse velocity analysis of co-moving stars, each corresponding to IL Cep and HD 216658. Being the most massive star in the region, HD 216658 should be the predominant excitation source, which created

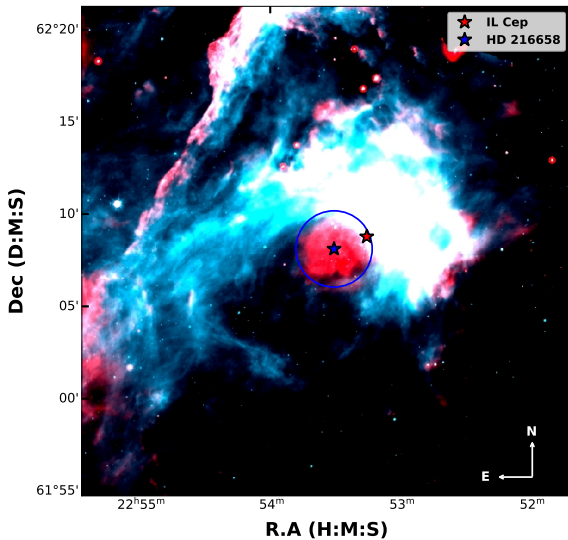
the cavity. Deharveng et al. (2010) noticed that the infrared bubble-like structures created by OB stars can be traced by the  $8 \mu\text{m}$  emission due to polycyclic aromatic hydrocarbon (PAH) molecules. Also, one can see  $24 \mu\text{m}$  emission in the central regions of the bubble, which is due to the emission from the dust grains. Deharveng et al. (2010), using *Spitzer*  $8 \mu\text{m}$  (IRAC 4) and  $24 \mu\text{m}$  (MIPS 1) images, pointed out that the bubbles/cavity can be traced by the  $8 \mu\text{m}$  images which shows PAH dominated emissions and the central source is associated with  $24 \mu\text{m}$  warm dust emission around it.

Figure 5 shows the *Spitzer* color composite image of the region around IL Cep, similar to the images generated by Deharveng et al. (2010). The figure shows both  $8 \mu\text{m}$  and  $24 \mu\text{m}$  emissions. We calculated the Strömgren radius for HD 216658 assuming the spectral type of the star as B0V (Morgan et al. 1953; Garrison 1970). The radius is estimated to be 0.5 pc ( $\sim 124 \text{ arcsec}$ ), which is illustrated in the Figure 5. We can see a spherical distribution of  $24 \mu\text{m}$  emission inside the Strömgren radius. The region around HD 216658 could be an ionised region completely devoid of  $8 \mu\text{m}$  PAH emission. This indicates that the predominant excitation source of the region is HD 216658, which may also be responsible for the creation of the cavity.

The astrometric solution of HD 216658 appears to be bad (RUWE = 2.7). But the star's geometrical position, association with a transverse velocity population which is identical to Cep OB3 stars, and the  $24 \mu\text{m}$  emission in its Strömgren radius show that HD 216658 is associated with the cavity and the Herbig Be star IL Cep.



**Figure 4.** The figure shows three histogram distributions. (1) The distance distribution of Cep OB3 stars taken from [Jordi et al. \(1995\)](#) (top). (2) The transverse velocities of Cep OB3 stars (bottom left). (3) The transverse velocities of co-moving stars of IL Cep (bottom right). The distribution of transverse velocities of the co-moving stars is bimodal with two distinct populations associated with IL Cep and HD 216658. The transverse velocity of both stars is shown using red and blue vertical lines. The two-gaussian fit gave the mean transverse velocity of both populations as  $8.3 \text{ km s}^{-1}$  and  $11.4 \text{ km s}^{-1}$ . The distance distribution peaks at 800 pc, which is similar to the co-moving members of IL Cep. Also, the transverse velocity distribution of the sample has a median value of  $11.6 \pm 0.6 \text{ km s}^{-1}$ . This is similar to the population of HD 216658.



**Figure 5.** The *Spitzer* color composite image of the region around HD 216658 created using  $8 \mu\text{m}$  (IRAC 4) emission in turquoise and  $24 \mu\text{m}$  (MIPS 1) in red. The Strömgren radius of HD 216658 is shown as a blue circle around HD 216658. The spherical distribution of  $24 \mu\text{m}$  emission inside the Strömgren radius indicates that the cavity is formed by HD 216658.

### 3.5 Coevality of co-moving stars from *Gaia* color-magnitude diagram

We identified 79 co-moving sources associated with IL Cep from the astrometric analysis of *Gaia* EDR3 data. The clustering of these stars around IL Cep suggests that they may have formed at the same time as IL Cep formed. Also, we found that there are two distinct transverse velocity populations in the co-moving stars. [Arun et al. \(2019\)](#) estimated the age of Herbig Be star IL Cep as  $0.11 \pm 0.1 \text{ Myr}$  from the isochrone fitting on the *Gaia* color-magnitude diagram. We used the *Gaia* photometric magnitudes ([Riello et al. 2020](#)) and distances ([Bailer-Jones et al. 2020](#)) for plotting the *Gaia* color-magnitude diagram (CMD) ( $G_{\text{RP}}$  vs  $M_G$ ) of the co-moving sources ([Kiman et al. 2019](#)). [Figure 6](#) shows the *Gaia* CMD of newly identified co-moving stars along with IL Cep and HD 216658. We have represented the subpopulations associated with IL Cep and HD216658 as separate symbols in the CMD to see whether they show any age difference. Modules for Experiments in Stellar Astrophysics (MESA) isochrones and evolutionary tracks (MIST)<sup>2</sup> of ages 0.1, 1, and 10 Myr ([Choi et al. 2016](#); [Dotter 2016](#)) along with low mass isochrone of 1 Myr from the CIFIST 2011\_2015<sup>3</sup> is plotted in the CMD. The *Gaia* CMD is not corrected for extinction. This will not affect the age estimates considerably since the interstellar extinction vector ( $A_V$ ) is approximately parallel to the isochrones, as shown in the [Figure 6](#). The CMD shows that majority of the co-moving stars are positioned above the 0.1 Myr isochrone. From the location of the co-moving stars in the

<sup>2</sup> <http://waps.cfa.harvard.edu/MIST>

<sup>3</sup> [https://phoenix.ens-lyon.fr/Grids/BT-Settl/CIFIST2011\\_2015/](https://phoenix.ens-lyon.fr/Grids/BT-Settl/CIFIST2011_2015/)

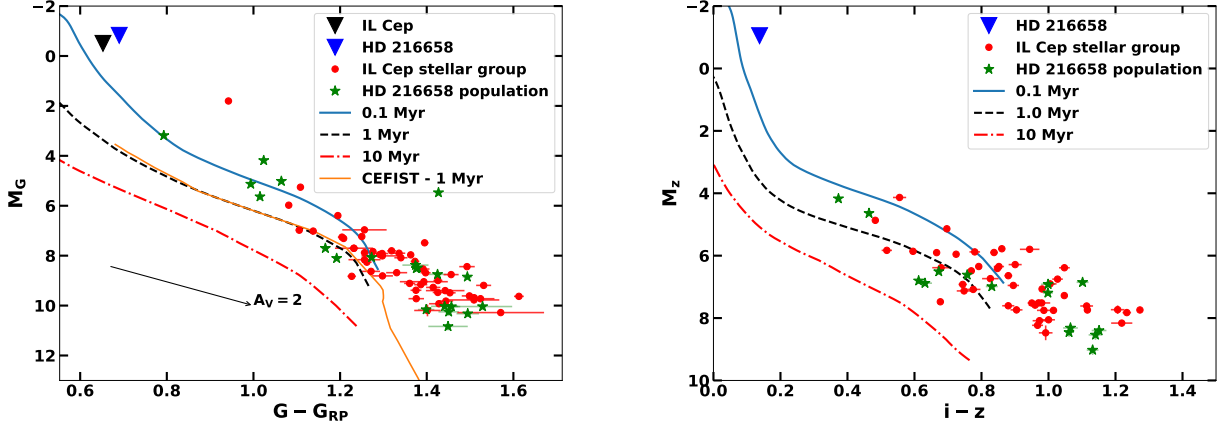


**Figure 6.** The Gaia EDR3 (left) and Pan-STARRS (right) CMD of the co-moving stars are illustrated. Most of the co-moving stars are identified to be coeval to IL Cep and are all indeed PMS stars in both CMD. IL Cep and HD 216658 are shown as black and blue star symbols respectively in the Gaia CMD. Only HD 216658 is shown in Pan-STARRS CMD.

CMD, it is identified that they are coeval to IL Cep. Most of the co-moving stars are positioned at regions slightly younger than IL Cep ( $> 0.1$  Myr). We may not be able to accurately estimate the ages of these stars.

Another optical CMD is created using Pan-STARRS DR1 (Chambers et al. 2016) photometric data to compliment the Gaia CMD. The coordinates of the co-moving stars are cross-matched with Pan-STARRS database with a 3" radius and got 78 matches. Avoiding stars without  $i$  and  $z$  magnitudes and also the stars with  $i$  and  $z$  magnitude uncertainty less than 0.02 mag are retained. The Pan-STARRS  $M_Z$  vs  $(i - z)$  color-magnitude diagram (CMD) of 62 stars satisfying the criteria shown in Figure 6 (right). The MIST isochrones of ages 0.1, 1, and 10 Myr are also shown. The Pan-STARRS CMD also shows that the co-moving stars are a younger population ( $\sim 0.1$  Myr). The  $i$  magnitude is not available for IL Cep. So only HD 216658 is also shown in the Pan-STARRS CMD.

The age of IL Cep estimated from this study using Gaia EDR3 matches with the previous estimates by Arun et al. (2019) using Gaia DR2 data. Also, from the CMD analysis, we found that the co-moving stars are coeval to IL Cep. The CMD analysis confirms that co-moving stars around IL Cep are PMS stars and most of them are formed at similar timescales as IL Cep. Interestingly, the brightest star in the region, HD 216658 is also occupying a similar position as IL Cep in the CMD. Also, from the present analysis, we do not find any distinction in ages between the sub-populations associated with HD 216658 and IL Cep.

### 3.6 Identification of circumstellar disk candidates

From the Gaia CMD analysis we found that all the co-moving stars are coeval with IL Cep and they are PMS stars in the age range 0.1 – 1 Myr. The stars with ages of a few Myr should be actively accreting from its circumstellar disk (Furlan et al. 2011; Semenov & Teague 2020). The accreting young stars will show infrared excess in their spectral energy distribution due to the thermal re-radiation from the dust in the circumstellar disk (Hillenbrand et al. 1992; Malfait et al. 1998). Saha et al. (2020) found that 80% of the co-moving stars around Herbig Be star HD 200775 are Class III objects. Thus it is important to identify the evolutionary phase of the co-moving stars

of IL Cep. With adequate infrared data, we can classify the young co-moving stars around IL Cep as embedded protostars (Class I), PMS stars with a circumstellar disk (Class II), and those that have already dissipated their accretion disks (Class III objects).

We extracted the 2MASS (Skrutskie et al. 2006) and *Spitzer* Glimpse 360 (Whitney et al. 2011) data of the co-moving stars of IL Cep. Glimpse 360 data contain IRAC [3.6] and IRAC [4.5] magnitudes but it does not include IRAC [5.8] and IRAC [8] magnitudes. The stars with 2MASS magnitudes with the quality flag ‘AAA’ and Glimpse 360 IRAC [3.6] and [4.5] magnitudes with uncertainty  $< 0.1$  mag are used for the identification of IR excess candidates. We selected 70 stars that satisfy the magnitude quality criteria. For the identification of IR excess candidates, we adopted the method developed by Gutermuth et al. (2008) using 2MASS JHK magnitudes and IRAC [3.6], [4.5] magnitudes. The method uses the T Tauri locus defined by Meyer et al. (1997) to find the intrinsic colors and the color constraints, which is explained in detail by Gutermuth et al. (2008). Using this method, we identified 25 stars as Class II objects and the remaining stars as Class III objects. The 2MASS H-K<sub>s</sub> vs J-H color-color diagram (CCDm) and the IR CCDm using  $([3.6] - [4.5])$  vs  $(K_s - [4.5])$  are shown in Figure 7. The stars of each sub-population among the co-moving stars are illustrated in the figure separately. The method adopted from Gutermuth et al. (2008) provided the  $A_V$  value relative to the T Tauri locus of all the Class II objects. The average extinction of the region is calculated as  $A_V = 3.7$  mag by taking the mean extinction of Class II sources. Also, we observe that 65% of all the co-moving stars are diskless sources (Class III). This observation is consistent with the findings of Saha et al. (2020) in the case of Herbig Be star HD 200775, where almost 80 % of the co-moving sources identified are Class III.

### 3.7 Identification of H $\alpha$ emission sources

The PMS stars are generally classified as T Tauri (Joy 1945) and H AeBe stars (Herbig 1960). The PMS stars have the common property of showing emission lines in their spectra (Hillenbrand et al. 1992). We classified the co-moving stars into Class II and Class III objects in the previous section. In this section, we identify H $\alpha$  emitting stars among the co-moving sources around IL Cep. We did

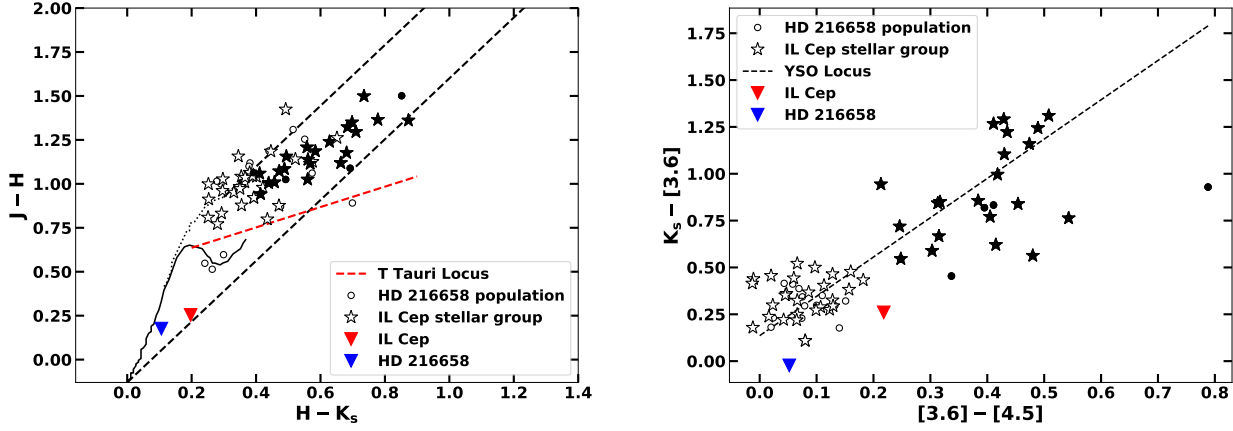


**Figure 7.** Figures show 2MASS and IR CCDm of co-moving stars of IL Cep. The HD 216658 population is shown as circles and IL Cep stellar group is marked as star symbols. The Class II sources among both populations are shown with filled black colors. The Class III sources are represented by non filled symbols. IL Cep and HD 216685 are also shown in both figures.

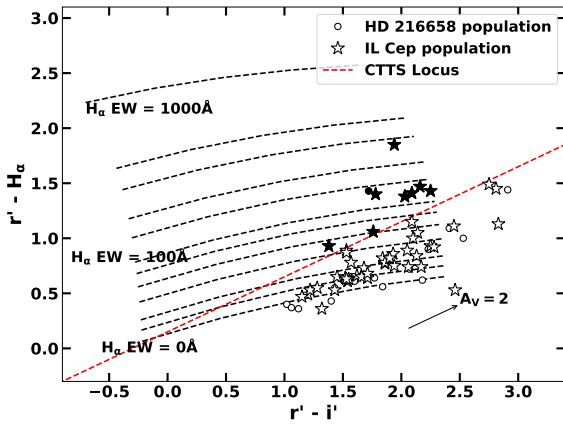


**Figure 8.** The figure shows the IPHAS CCDm with the synthetic  $H\alpha$  EW grid. The color-coding of the sources is similar to Figure 7. The dark-filled symbols are  $H\alpha$  sources identified in the study.

not avoid Class III objects for the analysis as there can be weak line T Tauri stars among the photometrically classified Class III objects. Also, [Saha et al. \(2020\)](#) identified Class III objects showing weak  $H\alpha$  emission from spectroscopy. We used the photometry from IPHAS ([Drew et al. 2005](#); [Barentsen et al. 2011](#)) which provides narrowband  $H\alpha$  photometry along with Sloan  $r'$  and  $i'$  magnitudes. We use IPHAS colors to construct CCDm for the identification of emission-line sources.

The IPHAS DR2 data for the stars are taken from the VizieR catalog services. We used a 3" search radius for all the co-moving stars associated with IL Cep for finding the IPHAS counterparts. If two detections are reported for a star, we took the closest one to the given coordinates. The IPHAS CCDm ( $r'-i'$ ) vs ( $r'-H\alpha$ ) is shown in Figure 8. The synthetic grid for various  $H\alpha$  emission equivalent width values are shown in Figure 8, which is adopted from [Drew et al. \(2005\)](#). We used the classical T Tauri star (CTTS) locus to

identify intense  $H\alpha$  emission sources ([Damiani et al. 2017](#); [Damiani 2018](#)). There are 9 sources above the CTTS locus, and they can be considered as confirmed  $H\alpha$  emission sources. All the 9 emission sources are classified as Class II sources in the infrared CCDm analysis in the previous section. All Class III sources and some Class II sources are below the CTTS locus. We may have missed some of the less intense  $H\alpha$  emission sources in the analysis. A thorough spectroscopic observation is required to identify less-intense  $H\alpha$  sources.

### 3.8 Spectroscopy and SED of bright stars

#### 3.8.1 IL Cep multiple system

IL Cep is reported to be an unresolved binary star by [Wheelwright et al. \(2010\)](#) and [Ismailov et al. \(2016\)](#). In this section, the star mentioned as IL Cep B (HD 216629B) is the visual binary companion of IL Cep ([Mel'Nikov et al. 1996](#)). For brevity, we will be mentioning IL Cep A as IL Cep in this work. The companion star IL Cep B is at a separation of 7" from the primary ([Gaia Collaboration et al. 2020](#)). The binary companion is also among the co-moving stars of IL Cep identified using Gaia EDR3 astrometric analysis (see Sect. 3.1). The star is the second brightest star in the co-moving group, the brightest being IL Cep itself. Both the stars being luminous and close to each other, IPHAS magnitudes are not listed in the archive and are not included in the emission line star identification analysis. We observed the optical spectra of IL Cep using the Himalayan Faint Object Spectrograph Camera (HFOSC) mounted on the 2-m Himalayan Chandra Telescope (HCT). The spectrum of IL Cep is reported in the study of [Mathew et al. \(2018\)](#), which discusses primarily about the  $O\text{I}$  lines in H AeBe stars rather than elaborating the spectral details of IL Cep. Further, we observed the spectrum of IL Cep B during our recent observation run using the OMR spectrograph (details are given in Sect. 2). It may be noted that although the spectra of both stars are taken with different spectrographs, the resolution is similar ( $\sim 8 \text{ \AA}$ ).

The  $H\alpha$  emission profiles of both stars are shown in Figure 9. The  $H\alpha$  emission is reported in IL Cep in various studies and the present data confirms the emission. Interestingly, we found that IL Cep B also shows emission in  $H\alpha$ . The measured  $H\alpha$  equivalent width (EW) of



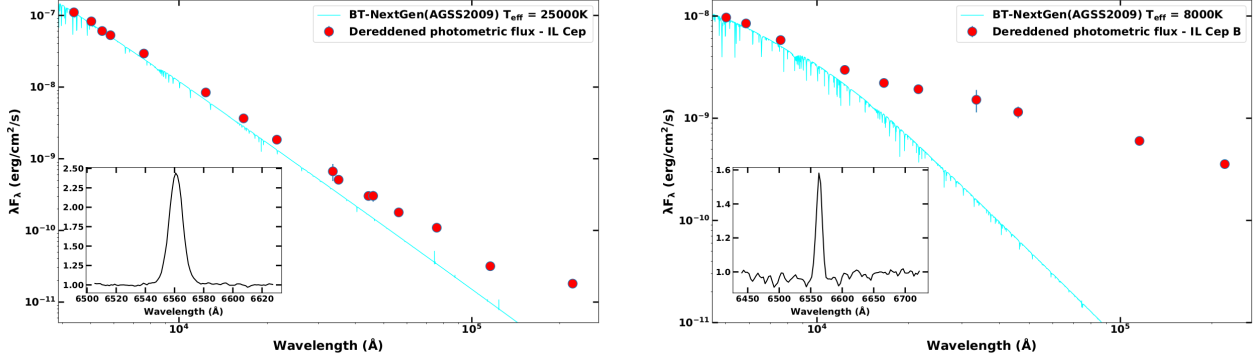


**Figure 9.** Figures show the best fit SEDs of IL Cep and IL Cep B. The BT-Next Gen (AGSS2009) synthetic spectra of fitted  $T_{\text{eff}}$  are shown. The  $H\alpha$  emission profiles of both stars are shown on the bottom left corners of each SED.

IL Cep and IL Cep B are  $-16^\circ$  and  $-7^\circ$ , respectively. The spectrum of IL Cep B has low SNR, making it difficult to estimate a proper spectral type. We constructed the SED of IL Cep and IL Cep B using the available magnitudes in optical and IR passbands. The magnitudes are extinction corrected with an  $A_V$  of 3.12 mag, taken from (Vioque et al. 2018). The IL Cep magnitudes in optical passbands are fitted (with chi-squared minimization) with a theoretical stellar atmosphere of effective temperature ( $T_{\text{eff}}$ ) 25000 K, at solar metallicity and for a surface gravity ( $\log g$ ) of 4.5. Similarly, for IL Cep B, the U, B, V magnitudes are fitted well with the stellar atmosphere corresponding to solar metallicity for  $T_{\text{eff}} = 8000$  K and  $\log g = 4.5$ . The spectral type is further validated from the temperature using the look-up table in Pecaut & Mamajek (2013). The spectral type of IL Cep is found to be B1.5, in agreement with the studies of Morgan et al. (1953) and Garrison (1970). IL Cep B is found to be an H Ae star of spectral type A6. The SEDs of both stars show IR excess, with IL Cep B showing higher flux excess than IL Cep. The spectral index (Lada index: Lada 1987; Greene et al. 1994) for both stars are estimated using 2MASS  $K_s$  and WISE W2 magnitudes ( $n_{2-4.6}$ ; Arun et al. 2019; Anusha et al. 2020). The  $n_{2-4.6}$  for IL Cep and IL Cep B are  $-2.4$  and  $-0.6$  respectively.

From the above discussion, we found that both the stars in the IL Cep binary system show  $H\alpha$  emission and IR excess, which are characteristic features of HAeBe stars. This classifies IL Cep to the rare class of binaries where one component is a Herbig Be star and the other is a Herbig Ae star.

### 3.8.2 HD 216658

The star HD 216658 is positioned at a similar location as IL Cep in the Gaia CMD. The star is identified to be the predominant excitation source in the region. The optical spectrum of HD216658 in the wavelength range 6000 – 7000 Å is shown in Figure 10. The star does not show any emission lines in the observed spectrum. The spectral type of HD 216658 is determined as B0V by comparing the absorption strength of He I 6678 Å with that of main sequence stars from the stellar library of Jacoby et al. (1984). This estimate is consistent with the previous spectral types reported in the literature, which is B0V - B0.5V (Morgan et al. 1953; Garrison 1970). Before performing the comparison, we normalized the spectra of HD 216658 and took the templates to a common resolution as the VBT spectra. The uncertainty in our spectral classification is found to be of two spectral subclasses. The age of IL Cep and other co-moving stars is

approximately 0.1 Myr. The spectral type being B0V, we estimated the PMS timescale of HD 216658 to be 0.03 Myr. If we assume that IL Cep stellar group is formed almost 0.1 Myr ago, HD 216658 completed its PMS evolutionary stage in at least 0.05 Myr and the inner disk must have got cleared in this timescale. This is consistent with the emission-less spectra for HD 216658. The SED fitted on the photometric data using the BT-NextGen model for HD 216658 is also shown in Figure 10. The star does not show IR excess till the WISE W3 band and a rise in SED is seen in the W4 band. The excess in W4 may be due to the IR emission from dust around HD 216658 (Sect. 3.4). However, it may be noted that the W4 magnitude is flagged as "d" in the WISE database, which means there is a possible diffraction spike on the observed image (Cutri et al. 2013). Hence, we cannot consider the excess in the W4 band to be real.

The star HD 216658 is found to be a member of the co-moving stars associated with IL Cep. The star is the most massive in the region and appears to be more evolved when compared to other co-moving stars, including IL Cep, and appears to have completed its PMS phase. Thus the star being more evolved and at a favorable position geometrically, it is safe to assume that HD 216658 is the initial trigger for the formation of the cavity in the region. IL Cep may have formed in the rims of the expanding cavity, along with the low mass co-moving stars.

### 3.9 Molecular clumps around IL Cep

The astrometric analysis has provided 78 co-moving stars associated with IL Cep, out of which 26 have been identified as IR excess candidates. The region appears to be having stars of age  $\sim 0.1$  Myr. Also, previous studies have shown that there are pre-stellar clumps on the edges of the expanding shell-like structure called the "cavity" (Zhang et al. 2016). This indicates that the region is very young and is still forming stars. Zhang et al. (2016) only studied the northern part of the cavity and identified 6 molecular clumps using  $^{13}\text{CO}(J=1-0)$  velocity-integrated intensity contours. To study all the regions around the cavity, especially the southern region, we use the  $\text{H}_2$  column density map generated using the Herschel maps in four bands (160 to 500  $\mu\text{m}$ ) (André et al. 2010; Marsh et al. 2015). We extracted the point process mapping (PPMAP)<sup>4</sup> data of  $25' \times 25'$  region around IL Cep, which covers the molecular cavity defined by Zhang et al.

<sup>4</sup> [http://www.astro.cardiff.ac.uk/research/ViaLactea/PPMAP\\_Results/](http://www.astro.cardiff.ac.uk/research/ViaLactea/PPMAP_Results/)

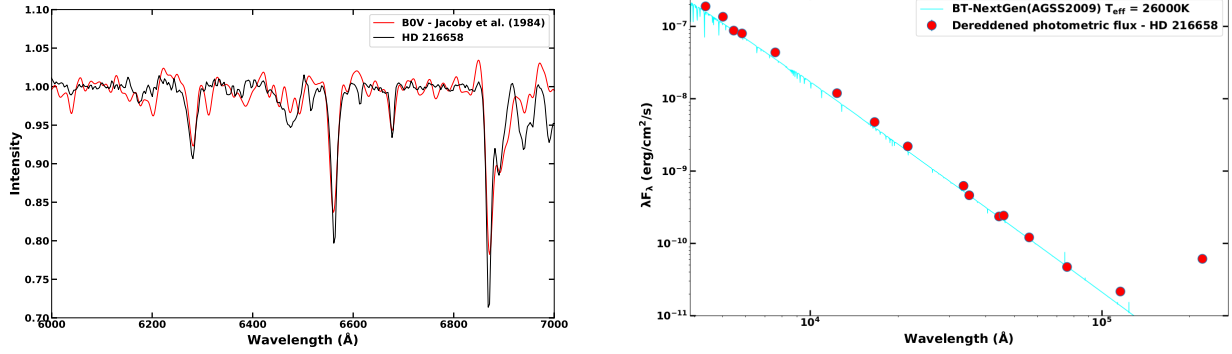


**Figure 10.** Figures show the optical spectrum (left panel) and SED (right panel) of HD 216658. The spectral type of the star is estimated to be B0V using [Jacoby et al. \(1984\)](#). The library spectra with spectral type B0V is also shown in the figure. The SED shows HD 216658 not having any near-IR excess.

(2016). The PPMAP has an angular resolution of 12" and a pixel scale of 6". To identify the clump-like structures in the region we used the dendrogram algorithm ([Goodman et al. 2009](#)). The dendrogram represents the hierarchy of the structures in any data. In our case, it is the  $H_2$  column density map. The python version of the algorithm *astrodendro* is implemented on the PPMAP to identify the structures on or around the cavity.

The *astrodendro* algorithm requires three input parameters for the implementation of the structure identification routine. The parameters are the lowest background (`min_value`), the lowest height of a structure (`min_delta`), and the minimum pixel size of a structure (`min_npix`). The `min_value` and `min_DELTA` are taken as  $3\sigma$  and  $1\sigma$ , which is  $35.7 \times 10^{20} \text{ cm}^{-2}$  and  $11.9 \times 10^{20} \text{ cm}^{-2}$  respectively ([Walker et al. 2021](#)). In order to identify a structure, we set a threshold of 5 pixels, in accordance with the PPMAP resolution ([Watkins et al. 2019](#)). Avoiding all the structures on the sides of the frame, we identified 11 structures on and around the cavity. The column density map and the identified clumps are shown in [Figure 11](#). Most of the northern structures we identified are consistent with the clumps identified by [Zhang et al. \(2016\)](#). Besides, we identified two clumps on the southern side of the cavity that was not identified in the previous studies. We estimated the total mass of each structure using the radius and  $N(H_2)$  values derived from the dendrogram algorithm. The coordinates, radius, and mass of the structures are listed in [Table 4](#). This implies that the ionization front created by the central star HD 216658 has compressed the northern and the southern regions. The gas content is considerably less towards the southern region of HD 216658. This may be the reason why relatively less clumping is seen in the southern region of the cavity.

### 3.10 Pressure effects due to HD 216658

HD 216658 is the primary source of UV photons in the region that carved out the "cavity". The high mass stars can exert pressure effects due to radiation ([Simón-Díaz & Stasińska 2008](#)), wind ([Dale et al. 2015](#)), and ionized gas ([Sternberg et al. 2003](#)) on the neighboring molecular clouds. In this section, we evaluate different pressure components by HD 216658 responsible for creating the cavity. The maximum radius of the cavity around the IL Cep region is 1.2 pc ([Zhang et al. 2016](#)). The variation of each of the pressure components from HD 216658 is evaluated up to 2 pc radius and is shown in [Figure 12](#). We compute the pressure due to stellar winds using the

**Table 4.** The table provides the coordinate offsets from HD 216658, radius and mass of 11 molecular clump-like structures identified in the dendrogram analysis.

Clump Number	R. A offset (arcsec)	Dec offset (arcsec)	Radius (pc)	Mass $M_\odot$
1	476.5	-164.8	0.04	19
2	564.9	-105.3	0.06	85
3	-309.0	-11.2	0.14	3016
4	-457.6	-80.7	0.05	46
5	151.6	278.9	0.05	94
6	87.9	263.6	0.03	6
7	-196.2	179.0	0.13	2551
8	-62.3	216.9	0.06	70
9	112.8	364.1	0.05	64
10	46.1	326.7	0.06	97
11	-88.5	534.1	0.05	44

following equation.

$$P_{wind} = \frac{M_W V_W}{4\pi D_s^2} \quad (1)$$

where  $M_W$  is the mass-loss rate,  $V_W$  is the stellar wind velocity and  $D_s$  is the distance from the star ([Baug et al. 2019](#)). We assumed an average mass loss rate of  $10^{-7} M_\odot \text{ yr}^{-1}$  and an average wind velocity of  $300 \text{ km s}^{-1}$  for HD 216658, assuming it as a HAeBe star in its PMS evolutionary stage ([Strafella et al. 1998](#)). We estimated the  $P_{wind}$  extended up to 2 pc using [Equation 1](#) by varying the  $D_s$  value. The pressure owing to the radiation ( $P_{rad}$ ) is computed using the equation.

$$P_{rad} = \frac{L_{bol}}{4\pi D_s^2} \quad (2)$$

The bolometric luminosity ( $L_{bol}$ ) of HD 216658 is estimated using V magnitude with necessary bolometric corrections.  $P_{rad}$  is estimated up to a radius of 2 pc and the pressure curve due to radiation is shown in [Figure 12](#).

Another component affecting the region is the pressure due to the ionized gas ( $P_{HII}$ ). The value of  $P_{HII}$  can be estimated using the expression given below.

$$P_{HII} = \mu_{II} m_H c_{II}^2 \left( \frac{S_{Lyc}}{4\pi\beta_2 D_s^3} \right)^{(1/2)} \quad (3)$$

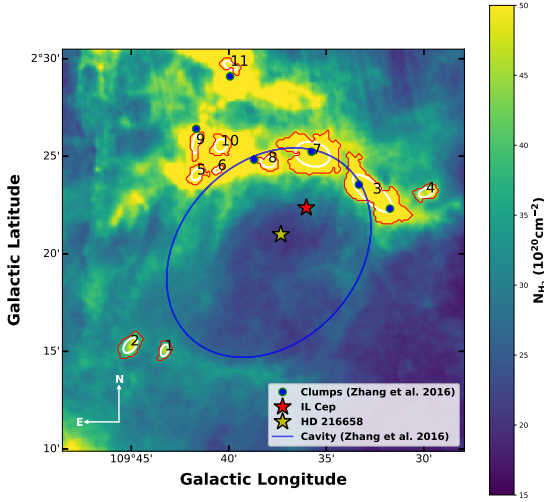


**Figure 11.** Figure illustrates the Herschel column density map taken from PPMAP. Dendrogram analysis identified 11 molecular clump-like structures on the expanding "cavity" around IL Cep. The structures on the northwest side are in agreement with the clumps identified by Zhang et al. (2016). Also, we have identified two additional clumps on the south-eastern region of IL Cep.

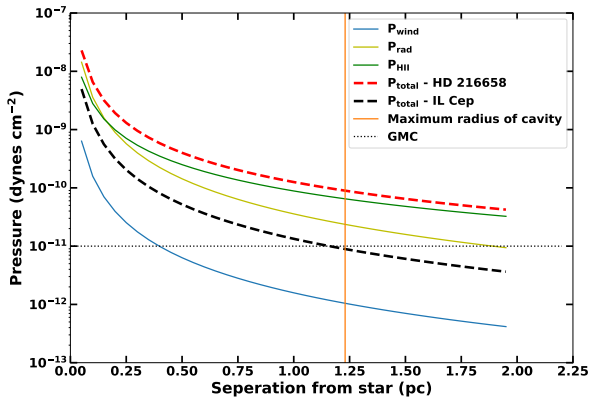


**Figure 12.** The figure shows various pressure components produced by HD 216658. The total pressure is shown using the red dashed line. The orange line is the maximum radius of the cavity. The pressure experienced by a GMC is shown by the black dotted line. The total pressure from the system is higher than normal GMC pressure at the maximum radius. The black dashed line shows the total pressure by IL Cep which is an order of magnitude lower than HD 216658. This shows that the HD 216658 itself is capable of producing the "cavity".

where, the mean molecular weight in an HII region,  $\mu_{\text{H}}=0.678$  (Bisbas et al. 2009), the sound speed in an HII region,  $c_{\text{H}}=11 \text{ km s}^{-1}$ , and the recombination coefficient,  $\beta_2=2.6 \times 10^{-13} \text{ cm}^3 \text{ s}^{-1}$ . Possible fluxes of Lyman Continuum Photons that is produced by a typical B0V-type progenitor ( $S_{\text{Lyc}} \sim 10^{47.3} \text{ photon s}^{-1}$ ) is taken from Panagia (1973). Considering all the parameters, we estimated  $P_{\text{HII}}$  value for IL Cep system upto a radius of 2 pc and is illustrated in the Figure 12. The figure is marked with the maximum radius of the cavity (1.2 pc). Also, the pressure experienced by a cool GMC (Giant Molecular Cloud) ( $10^{-11} \text{ dynes cm}^{-2}$ ; Baug et al. 2019) is shown in the Figure 12. A pressure approximately one order of magnitude higher than  $10^{-11} \text{ dynes cm}^{-2}$  produced by a source can perturb the region and eventually lead to cavity formation. We apply the similar analysis for the pressure components induced by IL Cep. The calculation is made by keeping wind pressure the same, but the  $L_{\text{bol}}$  and  $S_{\text{Lyc}}$  are changed for IL Cep accordingly. We find that the total exerted pressure is approximately an order of magnitude lower than HD 216658, and thus cannot be attributable for the observed cavity. The total pressure exerted by IL Cep is also shown in the Figure 12.

The analysis shows that HD 216658 system is producing enough pressure to create a cavity of radius 1.2 pc. The calculations are made on the assumption of its PMS nature and the present conditions. The protostellar stage of massive stars can be more violent and energetic, which shapes the expanding envelope around the star (Kuiper et al. 2015). Thus the pressure value is probably underestimated. Considering all the factors it is safe to argue that the cavity is indeed made by HD 216658.

### 3.11 Possible rocket effect by HD 216658 on the IL Cep co-moving association

The star forming regions are associated with infrared bubbles/cavities or molecular cloud structures (Churchwell et al. 2006; Deharveng et al. 2010). These cavity-like structures show an elevated star formation activity than other regions (Zhang & Wang 2012; Zhang et al. 2013). The cavity structures are created due to the pressure (wind & ionizing radiation) exerted by one or more OB type stars (Bertoldi 1989). The ionization front created by the expansion of the HII regions helps in the formation of bright rims on the boundaries of the cavity (Bedijn & Tenorio-Tagle 1984). These regions get accelerated by a process called "rocket effect" (Oort & Spitzer 1955). The clouds get displaced (cloud shuffling; Elmegreen 1979) by this acceleration (McKee & Ostriker 2007). This displacement due to the rocket effect is prominent on the surface facing the ionizing source (Getman et al. 2019). The next generation of stars formed in the accelerating clouds should possess the cloud's inherent motion, which can be traced by the proper motion of the stars (Dale et al. 2015).

We found that the B0V star HD 216658 is the source of excitation, thereby inducing the formation of a cavity. The Strömgren radius of the star is estimated as 0.5 pc and Figure 5 shows that the star IL Cep is at the boundary of the Strömgren radius of HD 216658. Zhang et al. (2016) shows that there are bright rims in the vicinity of IL Cep, which indicates a possible action of "rocket effect" on the region where IL Cep is formed. We have analysed the proposition that the star HD 216658 could have triggered a rocket effect on the surrounding region. IL Cep and the associated co-moving stars may have formed in the expanding cloud inheriting the motion imparted by the rocket effect.

The velocity difference between IL Cep stellar group and HD 216658 population in the sky plane is  $3.1 \text{ km s}^{-1}$  with a mean uncertainty of  $1.2 \text{ km s}^{-1}$  (see Sect. 3.3). The HD 216658 population has a transverse velocity of  $11.4 \text{ km s}^{-1}$  and the population is loosely

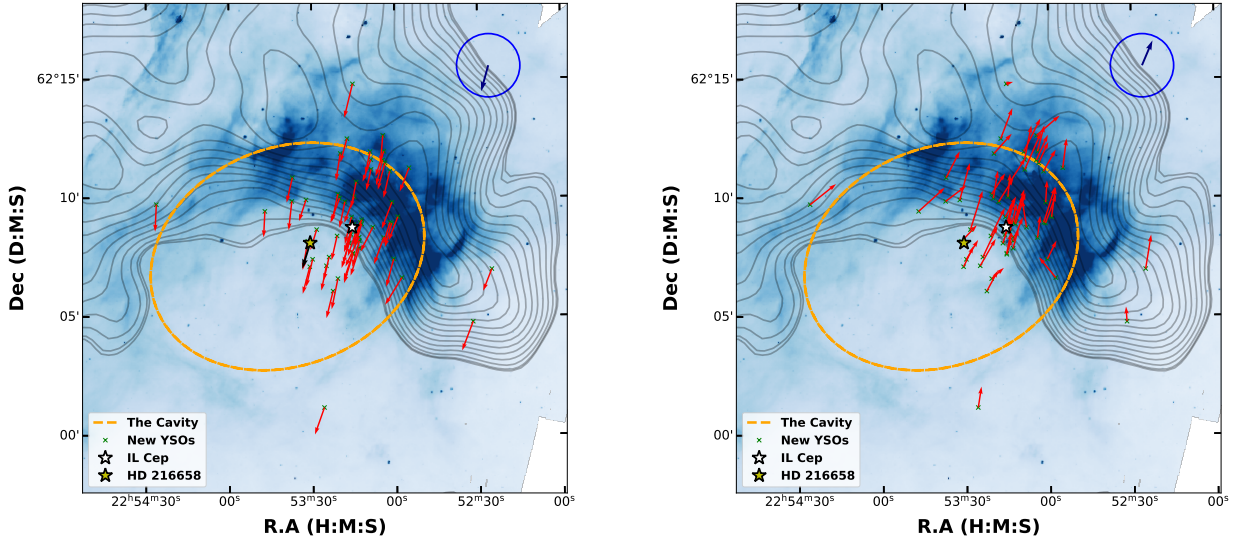


**Figure 13.** Figures show the IRAC  $8\ \mu\text{m}$  image of the IL Cep region with  $^{12}\text{CO}$  ( $J = 1-0$ ) channel map of  $-6$  to  $-9\ \text{km s}^{-1}$ . The proper motion vectors of the population of stars with a similar transverse velocity of IL Cep are shown in the figures. The left panel figure shows the normal proper motion vectors and the right panel figure has vectors after subtracting the proper motion of HD 216658. The median proper motion of all the stars is shown in the top right of both figures. The reversal of proper motion indicates to rocket effect by HD 216658 on IL Cep and the co-moving stars placed on the expanding cavity.

distributed all over the region of study. The HD 216658 population could be part of the bigger parent cloud Cep OB3. This indicates that the IL Cep stellar group with a transverse velocity of  $8.3\ \text{km s}^{-1}$  has been affected by a recoil force from the rocket effect, which in turn, reduced its transverse velocity. In other words, the PAH illuminated region (as traced by  $8\ \mu\text{m}$  IRAC map), where IL Cep is located expands with the plane-of-the-sky velocity of  $3\ \text{km s}^{-1}$ .

The argument that the IL Cep stellar group is formed due to the rocket effect caused by HD 216658 is illustrated using the proper motion vectors as well. The star HD 216658 can be considered as belonging to the first generation of stars formed in the region, having the original motion of the parent cloud Cep OB3. We subtracted the proper motion value of HD 216658 from all the stars in the IL Cep stellar group ( $> 10.3\ \text{km s}^{-1}$ ). Figure 13 shows the  $8\ \mu\text{m}$  (IRAC 4) image of the region with  $^{12}\text{CO}$  ( $J = 1-0$ ) channel map contours ( $-6$  to  $-9\ \text{km s}^{-1}$ ) from CGPS survey, observed using the FCRAO 14 m telescope. The left panel in Figure 13 shows the Gaia EDR3 proper motion before the subtraction of the proper motion of HD216658 and the right panel shows the proper motion subtracted vectors. The median proper motion vector of the stars is also shown in both figures. We see a reversal of proper motion for most of the co-moving candidates, thus mimicking an expansion. The reversal is more prominent for the stars in the PAH illuminated region, which is reported as the expanding structure. The  $^{13}\text{CO}$  channel map contours also indicate that the PAH illuminated region is having a velocity of  $-9\ \text{km s}^{-1}$ .

It is also worthwhile to note that the radial velocities of IL Cep and HD 216658 are reported as  $-39.40 \pm 2.00\ \text{km s}^{-1}$  and  $-27.50 \pm 3.40\ \text{km s}^{-1}$  respectively (Kharchenko et al. 2007). The minimum difference in the radial velocity of both stars is  $6.5\ \text{km s}^{-1}$ . The fact that IL Cep is having a faster radial velocity component than HD 216658 is a clear demonstration of the rocket effect.

We demonstrate using Gaia EDR3 data analysis that the Herbig

Be star IL Cep and its co-moving companions (IL Cep stellar group) were formed due to the triggered star formation by HD 216658 in the Cep OB3 association. This work may be one of the first observational demonstrations of the phenomenon of the "rocket effect" using astrometric data.

## 4 CONCLUSIONS

In this study, we report the clustered star formation inside the "cavity", around the Herbig Be star IL Cep. We used Gaia EDR3 astrometric data and other archival photometric surveys to find the accreting PMS stars among the co-moving stars. The major conclusions of the study are given below.

- The clustering of stars around IL Cep is identified using the Gaussian fitting of distance and proper motion values.
- The  $3 \times \text{WMAD}$  ellipses of  $d$  vs  $\mu_{\alpha*}$  and  $d$  vs  $\mu_{\delta}$  is used to find 78 stars that are co-moving with IL Cep.
- HD 216658, the brightest star that occupies the center of the "cavity" is identified to be the trigger for the formation of "cavity" and the co-moving sources using Gaia EDR3 astrometry.
- The histogram distribution of the transverse velocities of co-moving stars reveals two populations, each associated with IL Cep and HD 216658.
- The Gaia CMD indicates that most of the co-moving stars are co-eval with IL Cep. The stars are distributed around  $0.1\ \text{Myr}$  isochrones.
- The 2MASS and mid-IR CCDm are used to find IR excess candidates among the co-moving stars. We identified 25 stars as Class II sources.
- We found that 65 % of the co-moving stars in the IL Cep stellar group belong to Class III.
- From the spectral and SED analysis we found that IL Cep B is



a Herbig Ae star of A6 spectral type. This makes IL Cep a visual binary system where both components are HAeBe stars.

- Optical spectrum of HD 216658 shows no emission lines and has a spectral type of B0V. The star appears to be much more evolved than IL Cep and can be perceived as the initial trigger for "cavity" formation.

- We found 11 molecular clumps around IL Cep using dendrogram analysis.

- The total pressure exerted by HD 216658 on the surrounding region is calculated. The estimated pressure by the star is capable of creating the observed "cavity".

- The possibility of formation of IL Cep and co-moving stars by HD 216658 through rocket effect is discussed and demonstrated from the analysis of proper motion vectors.

## ACKNOWLEDGEMENTS

We would like to thank the referee for providing helpful comments and suggestions that improved the paper. R.A. thanks Ujjwal and Sudheesh for their valuable suggestions throughout the course of the work and also Newman College, Thodupuzha for providing facilities at the time of the pandemic. This work has made use of data from the European Space Agency (ESA) mission Gaia (<https://www.cosmos.esa.int/Gaia>), processed by the Gaia Data Processing and Analysis Consortium (DPAC; <https://www.cosmos.esa.int/web/Gaia/dpac/consortium>). Funding for the DPAC has been provided by national institutions, in particular, the institutions participating in the Gaia Multilateral Agreement. Also, we made use of the VizieR catalog access tool, Simbad and Aladdin, CDS, Strasbourg, France. The research has made use of the NASA/IPAC Infrared Science Archive, which is funded by the National Aeronautics and Space Administration and operated by the California Institute of Technology.

## DATA AVAILABILITY

The photometric and astrometric data are publicly available from the VizieR catalog<sup>5</sup>. The derived data generated in this research and the optical spectra will be shared on a reasonable request to the corresponding author.

## REFERENCES

André P., et al., 2010, *A&A*, **518**, L102  
 Anusha R., et al., 2020, *MNRAS*,  
 Arun R., Mathew B., Manoj P., Ujjwal K., Kartha S. S., Viswanath G., Narang M., Paul K. T., 2019, *AJ*, **157**, 159  
 Assousa G. E., Herbst W., Turner K. C., 1977, *ApJ*, **218**, L13  
 Bailer-Jones C. A. L., Rybizki J., Foesneau M., Mantelet G., Andrae R., 2018, *AJ*, **156**, 58  
 Bailer-Jones C. A. L., Rybizki J., Foesneau M., Demleitner M., Andrae R., 2020, arXiv e-prints, [p. arXiv:2012.05220](https://arxiv.org/abs/2012.05220)  
 Barentsen G., et al., 2011, *MNRAS*, **415**, 103  
 Baug T., de Grijs R., Dewangan L. K., Herczeg G. J., Ojha D. K., Wang K., Deng L., Bhatt B. C., 2019, *ApJ*, **885**, 68  
 Bedijn P. J., Tenorio-Tagle G., 1984, *A&A*, **135**, 81  
 Bertoldi F., 1989, *ApJ*, **346**, 735

Bisbas T. G., Wunsch R., Whitworth A. P., Hubber D. A., 2009, *A&A*, **497**, 649  
 Bisbas T. G., Whitworth A. P., Wunsch R., Hubber D. A., Walch S., 2011, in Alves J., Elmegreen B. G., Girart J. M., Trimble V., eds, IAU Symposium Vol. 270, Computational Star Formation. pp 263–266 ([arXiv:1007.2727](https://arxiv.org/abs/1007.2727)), doi:10.1017/S1743921311000482  
 Blaauw A., Hiltner W. A., Johnson H. L., 1959, *ApJ*, **130**, 69  
 Brodskaya E. S., 1953, Izvestiya Ordena Trudovogo Krasnogo Znameni Krymskoj Astrofizicheskoy Observatorii, **10**, 104  
 Castro-Ginard A., et al., 2020, *A&A*, **635**, A45  
 Chambers K. C., et al., 2016, arXiv e-prints, [p. arXiv:1612.05560](https://arxiv.org/abs/1612.05560)  
 Choi J., Dotter A., Conroy C., Cantiello M., Paxton B., Johnson B. D., 2016, *ApJ*, **823**, 102  
 Churchwell E., et al., 2006, *ApJ*, **649**, 759  
 Churchwell E., et al., 2007, *ApJ*, **670**, 428  
 Crawford D. L., Barnes J. V., 1970, *AJ*, **75**, 952  
 Cutri et al. 2013, VizieR Online Data Catalog, **2328**  
 Dale J. E., Haworth T. J., Bressert E., 2015, *MNRAS*, **450**, 1199  
 Damiani F., 2018, *A&A*, **615**, A148  
 Damiani F., Pillitteri I., Prisinzano L., 2017, *A&A*, **602**, A115  
 Deharveng L., et al., 2010, *A&A*, **523**, A6  
 Dotter A., 2016, *ApJS*, **222**, 8  
 Drew J. E., et al., 2005, *MNRAS*, **362**, 753  
 Elmegreen B. G., 1979, *ApJ*, **231**, 372  
 Fabricius C., et al., 2020, arXiv e-prints, [p. arXiv:2012.06242](https://arxiv.org/abs/2012.06242)  
 Fuente A., Martín-Pintado J., Bachiller R., Rodríguez-Franco A., Palla F., 2002, *A&A*, **387**, 977  
 Furlan E., et al., 2011, *ApJS*, **195**, 3  
 Gaia Collaboration Brown A. G. A., Vallenari A., Prusti T., de Bruijne J. H. J., Babusiaux C., Biermann M., 2020, arXiv e-prints, [p. arXiv:2012.01533](https://arxiv.org/abs/2012.01533)  
 Garmany C. D., 1973, *AJ*, **78**, 185  
 Garrison R. F., 1970, *AJ*, **75**, 1001  
 Getman K. V., Feigelson E. D., Kuhn M. A., Garmire G. P., 2019, *MNRAS*, **487**, 2977  
 Goodman A. A., Rosolowsky E. W., Borkin M. A., Foster J. B., Halle M., Kauffmann J., Pineda J. E., 2009, *Nature*, **457**, 63  
 Greene T. P., Wilking B. A., Andre P., Young E. T., Lada C. J., 1994, *ApJ*, **434**, 614  
 Gutermuth R. A., et al., 2008, *ApJ*, **674**, 336  
 Hamann F., Persson S. E., 1992, *ApJS*, **82**, 285  
 Herbig G. H., 1960, *ApJS*, **4**, 337  
 Heyer M. H., Brunt C., Snell R. L., Howe J. E., Schloerb F. P., Carpenter J. M., 1998, *ApJS*, **115**, 241  
 Hillenbrand L. A., Strom S. E., Vrba F. J., Keene J., 1992, *ApJ*, **397**, 613  
 Høg E., et al., 2000, *A&A*, **355**, L27  
 Ismailov N. Z., Khalilov O. V., Bakhaddinova G. R., 2016, *Astronomy Reports*, **60**, 265  
 Jacoby G. H., Hunter D. A., Christian C. A., 1984, *ApJS*, **56**, 257  
 Jordi C., Galadí-Enríquez D., Trullols E., Lahulla F., 1995, *A&AS*, **114**, 489  
 Joy A. H., 1945, *ApJ*, **102**, 168  
 Kharchenko N. V., Scholz R. D., Piskunov A. E., Röser S., Schilbach E., 2007, *Astronomische Nachrichten*, **328**, 889  
 Kiman R., Schmidt S. J., Angus R., Cruz K. L., Faherty J. K., Rice E., 2019, *AJ*, **157**, 231  
 Kuiper R., Yorke H. W., Turner N. J., 2015, *ApJ*, **800**, 86  
 Lada C. J., 1987, in Peimbert M., Jugaku J., eds, IAU Symposium Vol. 115, Star Forming Regions. pp 1–17  
 Lindegren L., et al., 2020, arXiv e-prints, [p. arXiv:2012.03380](https://arxiv.org/abs/2012.03380)  
 Magakian T. Y., 2003, *A&A*, **399**, 141  
 Malfait K., Bogaert E., Waelkens C., 1998, *A&A*, **331**, 211  
 Marsh K. A., Whitworth A. P., Lomax O., 2015, *MNRAS*, **454**, 4282  
 Mathew B., et al., 2018, *ApJ*, **857**, 30  
 McKee C. F., Ostriker E. C., 2007, *ARA&A*, **45**, 565  
 Mel'Nikov S. Y., Shevchenko V. S., Grankin K. N., Ibragimov M. A., Yakubov S. D., 1996, *Astronomy Reports*, **40**, 350  
 Merrill P. W., Burwell C. G., 1949, *ApJ*, **110**, 387  
 Meyer M. R., Calvet N., Hillenbrand L. A., 1997, *AJ*, **114**, 288

<sup>5</sup> <https://vizier.u-strasbg.fr/>

- Morau E., 2016, in EAS Publications Series. pp 73–114 ([arXiv:1607.00027](#)), doi:10.1051/eas/1680004
- Moreno-Corral M. A., C. C.-K., de La Ra E., Wagner S., 1993, *A&A*, **273**, 619
- Morgan W. W., Whitford A. E., Code A. D., 1953, *ApJ*, **118**, 318
- Morgan L. K., Thompson M. A., Urquhart J. S., White G. J., Miao J., 2004, *A&A*, **426**, 535
- Oort J. H., Spitzer Lyman J., 1955, *ApJ*, **121**, 6
- Panagia N., 1973, *AJ*, **78**, 929
- Pecaut M. J., Mamajek E. E., 2013, *ApJS*, **208**, 9
- Pozzo M., Naylor T., Jeffries R. D., Drew J. E., 2003, *MNRAS*, **341**, 805
- Prabhu T. P., Anupama G. C., Surendiranath R., 1998, Bulletin of the Astronomical Society of India, **26**, 383
- Riello M., et al., 2020, arXiv e-prints, p. [arXiv:2012.01916](#)
- Saha P., Gopinathan M., Kamath U., Lee C. W., Puravankara M., Mathew B., Sharma E., 2020, *MNRAS*, **494**, 5851
- Semenov D. A., Teague R. D., 2020, *Europhysics News*, **51**, 29
- Simón-Díaz S., Stasińska G., 2008, *MNRAS*, **389**, 1009
- Skrutskie M. F., et al., 2006, *AJ*, **131**, 1163
- Sternberg A., Hoffmann T. L., Pauldrach A. W. A., 2003, *ApJ*, **599**, 1333
- Strafella F., Pezzuto S., Corciulo G. G., Bianchini A., Vittone A. A., 1998, *ApJ*, **505**, 299
- Testi L., Palla F., Prusti T., Natta A., Maltagliati S., 1997, *A&A*, **320**, 159
- Testi L., Palla F., Natta A., 1998, *A&AS*, **133**, 81
- Testi L., Palla F., Natta A., 1999, *A&A*, **342**, 515
- The P. S., de Winter D., Perez M. R., 1994, *A&AS*, **104**, 315
- Vioque M., Oudmaijer R. D., Baines D., Mendigutía I., Pérez-Martínez R., 2018, *A&A*, **620**, A128
- Walker D. L., et al., 2021, arXiv e-prints, p. [arXiv:2102.03560](#)
- Waters L. B. F. M., Waelkens C., 1998, *ARA&A*, **36**, 233
- Watkins E. J., Peretto N., Marsh K., Fuller G. A., 2019, *A&A*, **628**, A21
- Wheelwright H. E., Oudmaijer R. D., Goodwin S. P., 2010, *MNRAS*, **401**, 1199
- Whitney B., et al., 2011, in American Astronomical Society Meeting Abstracts #217. p. 241.16
- Zhang C. P., Wang J. J., 2012, *A&A*, **544**, A11
- Zhang C. P., Wang J. J., Xu J. L., 2013, *A&A*, **550**, A117
- Zhang S.-J., Wu Y., Li J. Z., Yuan J.-H., Liu H.-L., Dong X., Huang Y.-F., 2016, *MNRAS*, **458**, 4222
- Zinnecker H., Yorke H. W., 2007, *ARA&A*, **45**, 481

Table 5: The table provides the relevant data of 78 co-moving stars of IL Cep.

Gaia EDR3 identifier	Offset from IL Cep (arcsec)	Distance (pc)	$\mu_{\alpha^*}$ (mas yr <sup>-1</sup> )	$\mu_{\delta}$ (mas yr <sup>-1</sup> )	G (mag)	G <sub>BP</sub> (mag)	G <sub>RP</sub> (mag)	Class
Gaia EDR3 2207203690787004800	7.7	780 <sup>+7</sup> <sub>-10</sub>	-0.68±0.02	-2.13±0.02	11.26	12.14	10.32	-
Gaia EDR3 2207203626363177344	15.1	715 <sup>+37</sup> <sub>-27</sub>	-0.68±0.07	-2.01±0.08	17.36	19.07	16.02	II
Gaia EDR3 2207203626363177984	18.9	788 <sup>+37</sup> <sub>-33</sub>	-0.68±0.06	-2.45±0.05	16.46	17.72	15.36	III
Gaia EDR3 2207203695082652928	23.8	811 <sup>+33</sup> <sub>-37</sub>	-0.58±0.06	-1.86±0.06	17.03	19.28	15.64	III
Gaia EDR3 2207109854345628544	25.2	892 <sup>+116</sup> <sub>-78</sub>	-0.58±0.11	-1.93±0.12	17.98	19.81	16.61	III
Gaia EDR3 2207203695077255808	25.6	822 <sup>+244</sup> <sub>-147</sub>	-0.56±0.24	-2.24±0.24	19.19	21.16	17.69	-
Gaia EDR3 2207203695082652544	30	783 <sup>+29</sup> <sub>-22</sub>	-0.64±0.04	-2.1±0.05	16.44	17.8	15.18	II
Gaia EDR3 2207109785619441792	31	718 <sup>+114</sup> <sub>-82</sub>	-1.14±0.18	-2.43±0.18	18.68	20.58	17.24	II
Gaia EDR3 2207109789917705344	39.3	763 <sup>+40</sup> <sub>-37</sub>	-0.59±0.07	-2.14±0.07	17.42	18.95	16.12	II
Gaia EDR3 2207191875332657664	41.2	750 <sup>+43</sup> <sub>-35</sub>	-0.62±0.08	-2.06±0.08	17.33	19.23	16.04	II
Gaia EDR3 2207191871033079680	44.3	792 <sup>+92</sup> <sub>-67</sub>	-0.46±0.16	-2.01±0.16	18.65	21.06	17.27	II
Gaia EDR3 2207109858637178624	51.9	785 <sup>+95</sup> <sub>-90</sub>	-1.02±0.16	-2.03±0.16	18.67	20.81	17.13	III
Gaia EDR3 2207109785619440000	56.2	778 <sup>+182</sup> <sub>-116</sub>	-0.72±0.26	-2.27±0.23	19.23	21.29	17.72	II
Gaia EDR3 2207191871033078272	66	786 <sup>+70</sup> <sub>-55</sub>	-0.76±0.09	-2.24±0.09	17.74	19.52	16.48	III
Gaia EDR3 2207203695082652032	66.7	761 <sup>+33</sup> <sub>-32</sub>	-0.44±0.06	-2.16±0.06	17.21	19.03	15.89	-
Gaia EDR3 2207098038883614080	68.6	702 <sup>+130</sup> <sub>-97</sub>	-0.75±0.25	-2.38±0.25	19.16	21.37	17.73	-
Gaia EDR3 2207203896941512960	77.1	809 <sup>+79</sup> <sub>-70</sub>	-0.82±0.12	-2.17±0.12	18.22	20.09	16.89	III
Gaia EDR3 2207203729442390528	79.9	774 <sup>+51</sup> <sub>-34</sub>	-0.75±0.07	-2.03±0.07	17.36	19.12	16.06	II
Gaia EDR3 2207109785619439744	81.4	780 <sup>+49</sup> <sub>-42</sub>	-1.11±0.08	-2.93±0.08	17.53	19.28	16.26	III
Gaia EDR3 2207203656423341440	82.8	910 <sup>+164</sup> <sub>-118</sub>	-0.57±0.16	-2.69±0.15	18.54	20.74	17.12	II
Gaia EDR3 2207109819979179904	83.8	707 <sup>+183</sup> <sub>-93</sub>	-0.8±0.21	-2.2±0.21	19.07	21.19	17.62	II
Gaia EDR3 2207203656423343744	84.8	815 <sup>+51</sup> <sub>-51</sub>	-0.25±0.1	-2.8±0.1	17.93	19.62	16.56	II
Gaia EDR3 2207191905392818816	90.1	875 <sup>+283</sup> <sub>-157</sub>	-0.52±0.23	-1.69±0.22	19.1	20.86	17.72	III
Gaia EDR3 2207203729442390272	91	819 <sup>+32</sup> <sub>-35</sub>	-0.48±0.05	-2.24±0.05	16.88	18.4	15.67	III
Gaia EDR3 2207191806607793792	95.6	864 <sup>+127</sup> <sub>-100</sub>	-0.45±0.2	-1.93±0.18	18.55	-	-	III
Gaia EDR3 2207110026137611520	96	826 <sup>+148</sup> <sub>-97</sub>	-0.54±0.16	-1.79±0.15	18.58	20.8	17.16	III
Gaia EDR3 2207098034588915840	99.2	766 <sup>+50</sup> <sub>-39</sub>	-1.03±0.08	-2.79±0.08	17.53	19.07	16.33	III
Gaia EDR3 2207191840972921344	100	829 <sup>+13</sup> <sub>-13</sub>	-1.04±0.02	-2.47±0.02	14.72	15.72	13.73	III
Gaia EDR3 2207110026144274304	100.2	803 <sup>+672</sup> <sub>-201</sub>	-0.56±0.33	-2±0.32	19.72	21.3	18.32	III
Gaia EDR3 2207203965660990592	114.7	858 <sup>+251</sup> <sub>-117</sub>	-0.42±0.2	-2.14±0.2	18.94	20.78	17.53	II
Gaia EDR3 2207191840967531904	115.7	836 <sup>+9</sup> <sub>-10</sub>	-1.55±0.01	-2.53±0.01	12.8	13.4	12	III
Gaia EDR3 2207191600449366784	117.4	704 <sup>+51</sup> <sub>-55</sub>	-0.42±0.15	-2.05±0.13	18.35	20.32	16.99	II
Gaia EDR3 2207191840974688768	117.8	732 <sup>+137</sup> <sub>-102</sub>	-0.42±0.34	-2.38±0.32	18.39	-	-	-
Gaia EDR3 2207110094866673536	118.2	808 <sup>+231</sup> <sub>-128</sub>	-0.77±0.24	-1.97±0.24	19.22	21.23	17.71	III
Gaia EDR3 2207110094856981632	118.5	746 <sup>+52</sup> <sub>-53</sub>	-0.85±0.11	-2.21±0.11	17.9	20.09	16.51	II
Gaia EDR3 2207191634809106816	128.3	843 <sup>+173</sup> <sub>-115</sub>	-1.09±0.19	-2.35±0.22	18.78	-	-	II
Gaia EDR3 2207191630514909184	129	821 <sup>+71</sup> <sub>-65</sub>	-0.53±0.13	-2.28±0.11	18.01	20.29	16.52	-
Gaia EDR3 220710975557965952	132	732 <sup>+31</sup> <sub>-27</sub>	-0.61±0.06	-2.31±0.06	17.03	18.65	15.79	II
Gaia EDR3 2207191596155045504	135	723 <sup>+70</sup> <sub>-53</sub>	-0.52±0.11	-2.54±0.1	17.93	19.67	16.65	II
Gaia EDR3 2207203759502525056	135.5	737 <sup>+56</sup> <sub>-64</sub>	-0.58±0.12	-1.75±0.11	18.15	20	16.85	II
Gaia EDR3 2207191634814494336	146.7	768 <sup>+16</sup> <sub>-14</sub>	-0.58±0.03	-2.24±0.02	15.4	16.59	14.32	III
Gaia EDR3 2207204721575215360	153.4	889 <sup>+354</sup> <sub>-203</sub>	-0.39±0.33	-1.74±0.34	19.47	21.29	17.94	II
Gaia EDR3 2207192042831672448	165.9	767 <sup>+65</sup> <sub>-59</sub>	-0.26±0.11	-2.39±0.11	18.11	20.49	16.71	III
Gaia EDR3 2207191531735280128	168.7	824 <sup>+43</sup> <sub>-33</sub>	-0.55±0.06	-2.24±0.06	16.81	18.52	15.56	III
Gaia EDR3 2207110958148796416	170.2	740 <sup>+26</sup> <sub>-24</sub>	-0.52±0.05	-2.21±0.05	16.6	18.14	15.4	II
Gaia EDR3 2207110953850443136	172.4	858 <sup>+242</sup> <sub>-205</sub>	-1.2±0.33	-2.34±0.37	19.7	21.14	18.26	II
Gaia EDR3 2207204721575140864	176.7	729 <sup>+54</sup> <sub>-58</sub>	-0.68±0.11	-1.83±0.11	18.14	19.8	16.91	III
Gaia EDR3 2207109648180096896	178.9	724 <sup>+170</sup> <sub>-141</sub>	-1.39±0.32	-2.25±0.42	19.58	21.21	18.01	II
Gaia EDR3 2207110958148795648	182.4	784 <sup>+15</sup> <sub>-11</sub>	-0.59±0.02	-2.23±0.02	14.73	15.98	13.62	III
Gaia EDR3 2207110953850289920	186.3	862 <sup>+44</sup> <sub>-41</sub>	-0.54±0.07	-2.1±0.08	17.38	18.9	16.15	III
Gaia EDR3 2207204000020636160	188.6	709 <sup>+57</sup> <sub>-54</sub>	-0.35±0.12	-2.27±0.12	18.01	20.28	16.55	II

Gaia EDR3 2207204794594275712	196.2	722 <sup>+34</sup> <sub>-33</sub>	-0.38±0.07	-1.86±0.07	17.13	18.84	15.85	III
Gaia EDR3 2207203798161868288	196.3	803 <sup>+44</sup> <sub>-33</sub>	-0.47±0.08	-2.07±0.08	17.69	19.32	16.43	III
Gaia EDR3 2207109961716390144	203.5	821 <sup>+238</sup> <sub>-163</sub>	-1.71±0.3	-2.52±0.32	19.61	21	18.16	III
Gaia EDR3 2207111125648971776	207.6	792 <sup>+183</sup> <sub>-124</sub>	-0.77±0.23	-1.98±0.24	18.97	20.96	17.54	III
Gaia EDR3 2207110953850296064	207.7	702 <sup>+77</sup> <sub>-65</sub>	-0.68±0.16	-2.07±0.17	18.72	21.06	17.27	-
Gaia EDR3 2207203866881344512	214.4	840 <sup>+64</sup> <sub>-71</sub>	-0.83±0.12	-2.92±0.11	18.14	20.12	16.76	III
Gaia EDR3 2207109686834905856	216.7	833 <sup>+96</sup> <sub>-93</sub>	-0.33±0.14	-2.87±0.15	18.51	-	-	III
Gaia EDR3 2207190771521448960	220.7	868 <sup>+433</sup> <sub>-197</sub>	-0.84±0.44	-2.95±0.39	19.94	21.45	18.49	III
Gaia EDR3 2207204755934881536	224	899 <sup>+200</sup> <sub>-111</sub>	-0.53±0.18	-1.94±0.18	18.81	20.84	17.42	II
Gaia EDR3 2207192356368997888	224.4	823 <sup>+32</sup> <sub>-32</sub>	-0.1±0.05	-2.15±0.05	16.59	17.93	15.45	III
Gaia EDR3 2207205000752704384	244.4	737 <sup>+19</sup> <sub>-14</sub>	-0.19±0.04	-2.26±0.04	15.73	17.08	14.54	III
Gaia EDR3 2207192081491094144	249.4	839 <sup>+59</sup> <sub>-43</sub>	-0.99±0.07	-2.53±0.06	17.32	18.84	16.16	III
Gaia EDR3 2207096900724266752	266.7	822 <sup>+289</sup> <sub>-303</sub>	-0.74±0.75	-3.11±0.75	20.41	22.12	18.96	III
Gaia EDR3 2207192352069321728	269.2	817 <sup>+11</sup> <sub>-11</sub>	-1.45±0.02	-2.51±0.02	14.57	15.67	13.51	III
Gaia EDR3 2207192425088470272	291.5	815 <sup>+7</sup> <sub>-8</sub>	-1.08±0.01	-2.57±0.01	13.74	14.77	12.72	III
Gaia EDR3 2207192425083076480	292.1	874 <sup>+114</sup> <sub>-82</sub>	-0.89±0.15	-2.78±0.14	18.19	20.02	16.81	III
Gaia EDR3 2207109510741529216	295.7	855 <sup>+267</sup> <sub>-169</sub>	-1.24±0.4	-2.51±0.52	19.98	21.38	18.49	III
Gaia EDR3 2207204893373835904	301.1	777 <sup>+200</sup> <sub>-160</sub>	-0.29±0.4	-2.91±0.33	19.49	21.79	17.96	II
Gaia EDR3 2207192115850832768	340.9	804 <sup>+11</sup> <sub>-14</sub>	-1.15±0.02	-2.59±0.02	15.16	16.19	14.15	-
Gaia EDR3 2207205103831917312	362.1	731 <sup>+145</sup> <sub>-109</sub>	-0.68±0.22	-2.8±0.22	18.95	21.29	17.34	III
Gaia EDR3 2207110301015137536	368.1	823 <sup>+227</sup> <sub>-133</sub>	-0.72±0.24	-1.84±0.27	19.3	20.88	17.93	III
Gaia EDR3 2207205168251744640	383.9	803 <sup>+194</sup> <sub>-100</sub>	-1.62±0.17	-3.22±0.17	18.37	20.51	16.88	III
Gaia EDR3 2207109270222912512	387.4	771 <sup>+53</sup> <sub>-45</sub>	-0.92±0.09	-2.42±0.08	17.34	19.17	16	III
Gaia EDR3 2207187541706040832	416.9	823 <sup>+322</sup> <sub>-221</sub>	-1.81±0.38	-2.46±0.32	19.74	21.37	18.34	III
Gaia EDR3 2207205550508517760	427.7	804 <sup>+19</sup> <sub>-24</sub>	-1.19±0.04	-2.8±0.04	15	17.49	13.57	III
Gaia EDR3 2207093572121225728	461.2	837 <sup>+64</sup> <sub>-68</sub>	-0.79±0.12	-2.23±0.09	17.58	19.65	16.22	III
Gaia EDR3 2207192901825130752	498.3	882 <sup>+56</sup> <sub>-58</sub>	-0.1±0.09	-2.24±0.08	17.61	19.28	16.35	III

This paper has been typeset from a  $\text{\LaTeX}$  file prepared by the author.